

Casson hybrid nanofluid flow over a Riga plate for drug delivery applications with double diffusion

Abeer S. Alnahdi and Taza Gul

Citation: Chin. Phys. B, 2024, 33 (**10**): 104701. DOI: 10.1088/1674-1056/ad624e
Journal homepage: http://cpb.iphy.ac.cn; http://iopscience.iop.org/cpb

What follows is a list of articles you may be interested in

Effect of viscosity on stability and accuracy of the two-component lattice Boltzmann method with a multiple-relaxation-time collision operator investigated by the acoustic attenuation model

Le Bai(柏乐), Ming-Lei Shan(单鸣雷), Yu Yang(杨雨), Na-Na Su(苏娜娜), Jia-Wen Qian(钱佳文), and Qing-Bang Han(韩庆邦)
Chin. Phys. B, 2022, 31 (**3**): 034701. DOI: 10.1088/1674-1056/ac2b93

Investigation of hypersonic flows through a cavity with sweepback angle in near space using the DSMC method

Guangming Guo(郭广明), Hao Chen(陈浩), Lin Zhu(朱林), and Yixiang Bian(边义祥)
Chin. Phys. B, 2021, 30 (**7**): 074701. DOI: 10.1088/1674-1056/abf7ad

Flow characteristics of supersonic gas passing through a circular micro-channel under different inflow conditions

Guang-Ming Guo(郭广明), Qin Luo(罗琴), Lin Zhu(朱林), Yi-Xiang Bian(边义祥)
Chin. Phys. B, 2019, 28 (**6**): 064702. DOI: 10.1088/1674-1056/28/6/064702

A new kind of hairpin-like vortical structure induced by cross-interaction of sinuous streaks in turbulent channel

Jian Li(李健), Gang Dong(董刚), Hui Zhang(张辉), Zhengshou Chen(陈正寿), Zhaode Zhang(张兆德)
Chin. Phys. B, 2018, 27 (**8**): 084701. DOI: 10.1088/1674-1056/27/8/084701

Three-dimensional turbulent flow over cube-obstacles

Hao Lu(卢浩), Wen-Jun Zhao(赵文君), Hui-Qiang Zhang(张会强), Bing Wang(王兵), Xi-Lin Wang(王希麟)
Chin. Phys. B, 2017, 26 (**1**): 014703. DOI: 10.1088/1674-1056/26/1/014703

Casson hybrid nanofluid flow over a Riga plate for drug delivery applications with double diffusion

Abeer S. Alnahdi[1,†] and Taza Gul[2,3,‡]

[1] *Department of Mathematics and Statistics, Faculty of Science, Imam Mohammad Ibn Saud Islamic University (IMSIU), Riyadh, Saudi Arabia*
[2] *Department of Mathematics, City University of Science and Information Technology, 25000, Peshawar, Pakistan*
[3] *DGoST- Directorate General of Science &Technology, Khyber Pakhtunkhwa, Peshawar, Pakistan*

(Received 9 March 2024; revised manuscript received 30 June 2024; accepted manuscript online 12 July 2024)

Casson fluid-mediated hybrid nanofluids are more effective at transferring heat than traditional heat transfer fluids in terms of thermal conductivity. Heat exchangers, cooling systems and other thermal management systems are ideal for use with Casson fluids. Precise control of the flow and release of medication is necessary when using Casson fluids in drug delivery systems because of their unique rheological properties. Nanotechnology involves the creation of nanoparticles that are loaded with drugs and distributed in Casson fluid-based carriers for targeted delivery. In this study, to create a hybrid nanofluid, both single-walled carbon nanotubes (SWCNTs) and multi-walled carbon nanotubes (MWCNTs) are dispersed in a Casson fluid with Fourier's and Fick's laws assumptions. The Casson fluid is suitable for various engineering and medical applications due to the enhancement of heat transfer and thermal conductivity by the carbon nanotubes. Our objective is to understand how SWCNTs and MWCNTs impact the flow field by studying the flow behavior of the Casson hybrid nanofluid when it is stretched against a Riga plate. The Darcy–Forchheimer model is also used to account for the impact of the porous medium near the stretching plate. Both linear and quadratic drag terms are taken into account in this model to accurately predict the flow behavior of the nanofluid. In addition, the homotopy analysis method is utilized to address the model problem. The outcomes are discussed and deliberated based on drug delivery applications. These findings shed valuable light on the flow characteristics of a Casson hybrid nanofluid comprising SWCNTs and MWCNTs. It is observed that the incorporation of carbon nanotubes makes the nanofluid a promising candidate for medical applications due to its improved heat transfer properties.

Keywords: carbon nanotubes (CNTs), Riga plate, Casson fluid with Fourier's and Fick's laws, analytical solutions

PACS: 47.27.nd, 47.15.gm, 44.15.+a **DOI:** 10.1088/1674-1056/ad624e

1. Introduction

The unique properties of carbon nanotubes (CNTs), including their high strength, flexibility, electrical conductivity and thermal conductivity, have led to their widespread applications in various industries. The typical diameter of CNTs is between 1 nm and 50 nm and they can be up to several micrometers long.[1] The size of nanoparticles can vary based on the method of synthesis used and any post-processing steps that are performed. CNTs are employed to create lightweight and sturdy materials for aircraft and spacecraft components.[2,3] Improving the structural integrity of these components leads to better performance and fuel efficiency. The production of electronic devices, such as transistors, sensors and touch screens, involves the use of CNTs. Performance enhancement of electronic components is made possible by the excellent electrical conductivity and high electron mobility of CNTs. High-performance batteries and supercapacitors have been developed using CNTs, which with their high surface area and excellent electrical conductivity can increase energy storage capacity and efficiency.[4] The automotive industry utilizes CNTs to create lightweight and strong materials for vehicle components such as body panels, chassis and batteries. This contributes to the enhancement of fuel efficiency and vehicle performance.

Drug delivery systems, tissue engineering and medical imaging are just a few of the biomedical applications that utilize CNTs. These applications are made possible by the biocompatibility of CNTs and their ability to penetrate cell membranes.[5] The addition of CNTs to a base fluid can enhance fluid properties because of their exceptional mechanical, thermal and electrical properties. Complex flow behavior can be described using the Casson fluid model, which is a non-Newtonian model that accounts for yield stress and fluid viscosity. Blood-borne drug carriers that target drug delivery systems are facilitated by the potential and widespread use of CNTs.[6] Their distinctive structure makes them a promising candidate for drug delivery applications due to their efficient loading and controlled release of therapeutic molecules. Furthermore, CNTs have been demonstrated to have low toxicity and are highly biocompatible, making them ideally suited for use in the bloodstream without causing harm to the body.[7,8] Targeted delivery to specific tissues or organs is made possi-

†Corresponding author. E-mail: asalnahdi@imamu.edu.sa
‡Corresponding author. E-mail: tazagul@cusit.edu.pk

© 2024 Chinese Physical Society and IOP Publishing Ltd

ble by the ability of CNTs to easily penetrate cell membranes; this minimizes side effects and improves treatment efficacy. The field of drug delivery and patient outcomes could be revolutionized by the use of CNTs as blood-borne drug carriers.[9]

Riga plates are suitable for use in drug delivery systems due to their high surface area and unique properties. Hybrid nanofluids (HNFs) can improve the dispersibility and stability of the drug by combining with CNTs, improving therapeutic efficacy.[10] CNTs are excellent for drug delivery because of their high aspect ratio, high surface area and strong mechanical properties. By utilizing Riga plates in CNT-based nanofluids, the drug carrier system can be improved to release drugs and deliver them to specific tissues or organs with controlled release.[11,12] The use of Riga plates in drug carriers with CNT HNFs is a promising way to improve drug delivery systems and advance nanomedicine. New and improved drug delivery strategies for various medical applications could be developed through further research and development in this area.[13]

The use of Darcy–Forchheimer model in drug delivery using CNT HNFs is crucial because it can improve the transport properties of drug-loaded nanofluids through porous media. Researchers can accurately predict drug transport characteristics and optimize the delivery process by using the Darcy–Forchheimer equation to describe the flow behavior of nanofluids in porous media.[14] In addition, the Darcy–Forchheimer model facilitates understanding of the connection between the CNTs and the drug molecules, providing insight into the diffusion and release processes within the nanofluid. The design of efficient drug delivery systems that can effectively target specific tissues or organs is crucial for improving therapeutic outcomes. The Darcy–Forchheimer model is indispensable for examining and optimizing the drug delivery procedure with CNT HNFs. The development of advanced drug delivery systems with improved efficiency and efficacy is assisted by a comprehensive understanding of transport phenomena.[15] In various physical systems, including environmental processes and industrial applications, the transport of energy and mass is crucial. Analysis of this transport frequently involves using a generalized form of the Fourier energy flux equation and Fick's mass flux equation.[16] A temperature gradient leads to the flow of thermal energy through a material, as described by Fourier's law of heat conduction. The heat transfer process is significantly modified by incorporating the effects of a magnetic field.[17,18] Magneto-thermal convection and magneto-enhanced thermal conductivity are two additional heat transfer mechanisms that can occur when a magnetic field is present, and can induce Lorentz forces. The transport of mass through a material due to a concentration gradient is governed by it, similar to Fick's law of diffusion. Magnetophoresis can affect the mass transport process when there a magnetic field is present, as magnetic forces drive particle motion.[19,20] A complete understanding of energy and mass transport can be achieved when a magnetic field is combined with Fourier's and Fick's equations. Complex transport phenomena with important implications for various fields of study can arise from the interaction between thermal and concentration gradients and magnetic fields. Optimizing performance in a variety of technological applications, such as magnetic refrigeration systems and drug delivery devices, requires us to understand and control these transport processes.[21] Electromagnetic HNFs offer several advantages when used in drug delivery applications.[22] The ability to remotely control the flow of nanofluids through the body using an external magnetic field is a significant benefit. Targeted and precise delivery of drugs to specific sites in the body is made possible by this, resulting in a reduction in side effects and improved efficacy.[23] In addition, nanofluids contain electromagnetic particles that can serve as drug carriers, allowing for sustained release over time.[24,25] The use of electromagnetic HNFs for drug delivery can be challenging due to the need for stable and efficient flow through the body. In this study we address this challenge by proposing a Riga flow system. A microchannel that has grooves on the walls is used in a Riga flow system to create vortices that help with the mixing and dispersion of nanofluids. By improving the circulation and distribution of nanoparticles throughout the body, this system increases the effectiveness of the drug delivery process.[27] A Riga flow system can improve the flow of electromagnetic HNFs for drug delivery applications by controlling their size, concentration and surface properties. Researchers can ensure efficient drug delivery with minimal side effects by fine-tuning these parameters to improve the carriers' stability, biocompatibility and drug-carrying capacity.[28]

The significance of the homotopy analysis method (HAM) in solving fluid flow problems lies in its capacity to provide precise and efficient solutions to complex nonlinear equations.[29,30] This method can help researchers and engineers gain valuable insights into fluid behavior in different systems and optimize their designs for improved performance and efficiency. Additionally, the HAM can also contribute to the development of new analytical tools and approaches for studying fluid dynamics, which can contribute to advances in the field of fluid mechanics.[31,32]

We highlight the novelty of this study based on the above discussion. The base fluid for drug delivery applications with a Casson fluid is an HNF made up of single-walled CNTs (SWCNTs) and multi-walled CNTs (MWCNTs). Drug delivery applications involve the assumption of electromagnetic flow on a Riga plate. Double diffusion is included in the Cattaneo–Christov thermal flux model, in contrast to the conventional Fourier equation. Both thermophoretic and Brownian motion are present in the Darcy–Forchheimer model.

2. Mathematical formulation

To investigate drug delivery, the problem statement for a CNT HNF flow on a Riga plate is formulated. External electromagnetic forces are used to model the flow behavior of CNT nanofluids. This study focuses on the movement of a CNT HNF through a Casson base fluid over a Riga plate while under an electromagnetic field. The objective is to assess the impact of the electromagnetic field on the flow and heat transfer characteristics of the nanofluid, along with its corresponding velocity and temperature profiles. The Riga stretched plate velocity is $u_{\mathrm{w}}(x) = ax$ along the x-axis. T_{w} and C_{w} are the wall surface temperature and concentration, respectively. The ambient temperature and concentration are T_∞ and C_∞, respectively. Fourier's and Fick's laws are also assumed in the model problem. Assumptions from the Darcy–Forchheimer model are employed to model the flow field. The flow field is restricted to laminar, preventing the effects of turbulence.

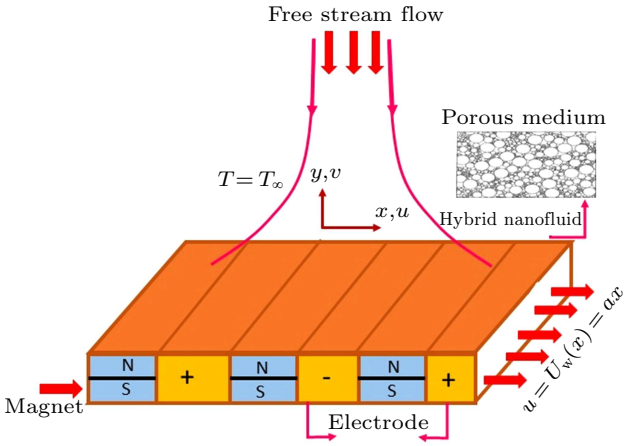


Fig. 1. The geometry of the proposed model.

Under the assumptions mentioned above, the basic governing equations are defined as

$$u_x + v_y = 0, \tag{1}$$

$$\begin{aligned}&\rho_{\mathrm{hnf}}\left(uu_x + vu_y\right)\\ &= \left(1+\beta^{-1}\right)\upsilon_{\mathrm{hnf}}u_{yy} + \frac{\pi j_0 M^*}{8}\exp\left(-\frac{\pi}{a_1}y\right)\\ &\quad - \frac{\mu_{\mathrm{hnf}}}{K^*}\left(1+\beta^{-1}\right)u - F_0u^2 - \sigma_{\mathrm{hnf}}\left(E_0B_0 - B_0^2u\right),\end{aligned} \tag{2}$$

$$\begin{aligned}&\left(\rho c_p\right)_{\mathrm{hnf}}\left(uT_x + vT_y + \tau_{\mathrm{e}}\Lambda_T\right)\\ &= k_{\mathrm{hnf}}T_{yy} + \tau\left[\frac{D_T}{T_\infty}\left(T_y\right)^2 + D_B\left(T_yC_y\right)\right]\\ &\quad + \sigma_{\mathrm{hnf}}\left(uB_0 - E_0\right)^2 + Q(T - T_\infty),\end{aligned} \tag{3}$$

$$\begin{aligned}&uC_x + vC_y + \tau_{\mathrm{m}}\Lambda_C\\ &= D_{\mathrm{hnf}}C_{yy} + \frac{D_T}{T_\infty}\left(T_{yy}\right) + Kr(C - C_\infty),\end{aligned} \tag{4}$$

where

$$\begin{aligned}\Lambda_T &= uu_xT_x + uv_xT_y + vv_yT_y + vu_yT_x + u^2T_{xx}\\ &\quad + 2uvT_{xy} + v^2v_xT_{yy},\\ \Lambda_C &= uu_xC_x + uv_xC_y + vv_yC_y + vu_yC_x + u^2C_{xx}\\ &\quad + 2uvC_{xy} + v^2v_xC_{yy},\end{aligned} \tag{5}$$

along with the boundary conditions

$$\begin{aligned}&u(0) = ax = U_{\mathrm{w}}(x), \quad v(0) = 0,\\ &T(0) - T_{\mathrm{w}} = 0, \quad C(0) - C_{\mathrm{w}} = 0,\\ &u(\infty) \to 0, \quad T(\infty) \to T_\infty, \quad C(\infty) \to C_\infty.\end{aligned} \tag{6}$$

Each component in the above equations is defined in the nomenclature in Appendix A.

Table 1. Thermophysical characteristics of hybrid nanofluids.

Nanoparticle relations
$\frac{\mu_{\mathrm{hnf}}}{\mu_{\mathrm{f}}} = (1-\phi_1)^{-2.5}(1-\phi_2)^{-2.5}, \quad \phi_{\mathrm{SWCNT}} = \phi_1, \quad \phi_{\mathrm{MWCNT}} = \phi_2,$
$\frac{\rho_{\mathrm{hnf}}}{\rho_{\mathrm{f}}} = (1-\phi_2)\left[(1-\phi_1) + \phi_1\left(\frac{\rho_1}{\rho_{\mathrm{f}}}\right)\right] + \phi_2\left(\frac{\rho_2}{\rho_{\mathrm{f}}}\right),$
$\frac{(\rho cp)_{\mathrm{hnf}}}{(\rho cp)_{\mathrm{f}}} = (1-\phi_2)\left[(1-\phi_1) + \phi_1\left(\frac{(\rho cp)_1}{(\rho cp)_{\mathrm{f}}}\right)\right] + \phi_2\left(\frac{(\rho cp)_2}{(\rho cp)_{\mathrm{f}}}\right),$
$\frac{k_{\mathrm{hnf}}}{k_{\mathrm{nf}}} = \left[(1-\phi_2) + 2\phi_2\left(\frac{k_2}{k_2-k_{\mathrm{nf}}}\right)\ln\left(\frac{k_2+k_{\mathrm{nf}}}{k_{\mathrm{nf}}}\right)\right]\left[(1-\phi_2) + 2\phi_2\left(\frac{k_{\mathrm{nf}}}{k_2-k_{\mathrm{nf}}}\right)\ln\left(\frac{k_2+k_{\mathrm{nf}}}{k_{\mathrm{nf}}}\right)\right]^{-1},$
$\frac{k_{\mathrm{nf}}}{k_{\mathrm{f}}} = \left[(1-\phi_1) + 2\phi_1\left(\frac{k_1}{k_1-k_{\mathrm{f}}}\right)\ln\left(\frac{k_1+k_{\mathrm{f}}}{k_{\mathrm{f}}}\right)\right]\left[(1-\phi_1) + 2\phi_1\left(\frac{k_{\mathrm{f}}}{k_1-k_{\mathrm{f}}}\right)\ln\left(\frac{k_1+k_{\mathrm{f}}}{k_{\mathrm{f}}}\right)\right]^{-1},$
$\frac{\sigma_{\mathrm{hnf}}}{\sigma_{\mathrm{f}}} = \left[\sigma_2 + 2\sigma_{\mathrm{nf}} - 2\left(\sigma_{\mathrm{nf}} - \sigma_2\right)\phi_2\right]\left[\sigma_2 + 2\sigma_{\mathrm{nf}} + \left(\sigma_{\mathrm{nf}} - \sigma_2\right)\phi_2\right]^{-1},$
$\frac{\sigma_{\mathrm{nf}}}{\sigma_{\mathrm{f}}} = \left[\sigma_1 + 2\sigma_{\mathrm{f}} - 2\left(\sigma_{\mathrm{f}} - \sigma_1\right)\phi_1\right]\left[\sigma_1 + 2\sigma_{\mathrm{f}} + \left(\sigma_{\mathrm{f}} - \sigma_1\right)\phi_1\right]^{-1}$

Table 2. The experimental findings concerning the solid particles and base fluid.

Material	Density ρ (kg·m^{-3})	Thermal conductivity k (W·mK^{-1})	Electrical conductivity σ (S·m^{-1})	Heat capacity c_p (J·kg^{-1}·K^{-1})
SWCNTs	2600	3.7	1.1×10^{7}	425
Blood	1053	0.492	5.5×10^{-6}	3594
MWCNTs	1600	3000	59.6×10^{6}	796

The relations between the thermophysical properties of the nanoparticles are given in Table 1 and the experimental values of these properties are given in Table 2.

In Table 1, ϕ_1 and ϕ_2 represent the concentration of SWCNTs and MWCNTs, respectively. The subscripts nf and hnf are used to show the corresponding properties of the nanofluid and HNF, respectively. Introducing the similarity variables

$$\begin{aligned}
&\eta = y\sqrt{a\upsilon_{\mathrm{f}}^{-1}}, \quad u = axf'(\eta),\\
&\Theta(\eta)(T_{\mathrm{w}}-T_{\infty}) = T-T_{\infty}, \quad v = -\sqrt{a\upsilon_{\mathrm{f}}}f(\eta),\\
&\varphi(\eta)(C_{\mathrm{w}}-C_{\infty}) = C-C_{\infty},
\end{aligned} \tag{7}$$

equations (1)–(7) transform as

$$\begin{aligned}
&\frac{\upsilon_{\mathrm{hnf}}}{\upsilon_{\mathrm{f}}}\left(1+\beta^{-1}\right)f'''(\eta) - f'(\eta)^2 + f(\eta)f''(\eta)\\
&-Fr\frac{\rho_{\mathrm{f}}}{\rho_{\mathrm{hnf}}}f'(\eta)^2 - \lambda\frac{\upsilon_{\mathrm{hnf}}}{\upsilon_{\mathrm{f}}}\left(1+\beta^{-1}\right)f'(\eta)\\
&-\frac{\sigma_{\mathrm{hnf}}/\sigma_{\mathrm{f}}}{\rho_{\mathrm{hnf}}/\rho_{\mathrm{f}}}M\left(E-f'(\eta)\right) + \frac{\rho_{\mathrm{f}}}{\rho_{\mathrm{hnf}}}\alpha\,\mathrm{e}^{(-B\eta)} = 0,
\end{aligned} \tag{8}$$

$$\begin{aligned}
&\frac{\alpha_{\mathrm{hnf}}}{\alpha_{\mathrm{f}}}\frac{1}{Pr}\Theta''(\eta) + \frac{\sigma_{\mathrm{hnf}}/\sigma_{\mathrm{f}}}{(\rho c_p)_{\mathrm{hnf}}/(\rho c_p)_{\mathrm{f}}}EcM\left(f'(\eta)-E\right)^2\\
&+f(\eta)\Theta'(\eta) + \frac{(\rho c_p)_{\mathrm{f}}}{(\rho c_p)_{\mathrm{hnf}}}\chi\Theta(\eta)\\
&+Nb\Theta'(\eta)\varphi'(\eta) + Nt\Theta'(\eta)^2 - \gamma_{\mathrm{e}}\chi_T = 0,
\end{aligned} \tag{9}$$

$$\begin{aligned}
&\frac{(1-\phi_1)(1-\phi_2)}{Sc}\varphi''(\eta) + \varphi'(\eta)f(\eta) - k_1\varphi(\eta)\\
&+\frac{Nt}{Nb}\Theta''(\eta) - \gamma_{\mathrm{m}}\chi_C = 0,
\end{aligned} \tag{10}$$

where

$$\begin{aligned}
\chi_T &= \frac{(\rho c_p)_{\mathrm{f}}}{(\rho c_p)_{\mathrm{hnf}}}\chi\Theta'(\eta) - \frac{\sigma_{\mathrm{hnf}}/\sigma_{\mathrm{f}}}{(\rho c_p)_{\mathrm{hnf}}/(\rho c_p)_{\mathrm{f}}}\\
&\quad\times EcM\left(f'(\eta)^2 + f''(\eta)f(\eta) - E\right)\\
&\quad+f(\eta)\Theta'(\eta)f'(\eta) + \Theta''(\eta)f(\eta)^2,\\
\chi_C &= f(\eta)\varphi'(\eta)f'(\eta) + \varphi''(\eta)f(\eta)^2\\
&\quad-k_1\varphi'(\eta)f(\eta)f'(\eta)\varphi'(\eta)\\
&\quad+\varphi''(\eta)f(\eta)^2 - k_1\varphi'(\eta)f(\eta),
\end{aligned} \tag{11}$$

with

$$\begin{aligned}
&f'(0) = 1, \quad \Theta(0) = 1, \quad f(0) = 0, \quad \varphi(0) = 1,\\
&f'(\infty) = 0, \quad \Theta(\infty) = 0, \quad \varphi(\infty) = 0.
\end{aligned} \tag{12}$$

The parameters in the above transform equations are defined as

$$\begin{aligned}
&Fr = \frac{xF_0}{\rho_{\mathrm{f}}}, \quad E = \frac{E_0}{B_0(U_{\mathrm{w}})}, \quad M = \frac{\sigma_{\mathrm{f}}B_0^2}{\rho_{\mathrm{f}}a},\\
&\lambda = \frac{\nu_{\mathrm{f}}}{ak^*}, \quad \alpha = \frac{j_0M^*\pi}{8a^2x\rho_{\mathrm{f}}},\\
&Pr = \frac{\upsilon_{\mathrm{f}}}{\alpha_{\mathrm{f}}}, \quad \gamma_{\mathrm{e}} = a\tau_{\mathrm{e}}, \quad \chi = \frac{Q}{(\rho c_p)_{\mathrm{f}}a},\\
&Ec = \frac{a^2x^2}{(c_p)_{\mathrm{f}}(T_{\mathrm{w}}-T_{\infty})}, \quad \gamma_{\mathrm{m}} = a\tau_{\mathrm{m}},\\
&Nt = \frac{\tau D_T(T_{\mathrm{w}}-T_{\infty})}{\upsilon_{\mathrm{f}}T_{\infty}}, \quad Sc = \frac{\upsilon_{\mathrm{f}}}{D_B},\\
&Nb = \frac{\tau D_B(C_{\mathrm{w}}-C_{\infty})}{\upsilon_{\mathrm{f}}}, \quad k_1 = \frac{kr}{a}.
\end{aligned} \tag{13}$$

Information about these parameters is given in the nomenclature.

The skin friction coefficient (C_{f}), Nusselt number (Nu) and Sherwood number (Sh) are the physical quantities connected to the behaviors of drag force, heat transfer and mass transfer. The simplified form of the above physical quantities is

$$\begin{aligned}
&Re_x^{\frac{1}{2}}Cf = f''(0), \quad Re_x^{-\frac{1}{2}}Sh = \varphi'(0),\\
&Re_x^{-\frac{1}{2}}Nu = -\frac{k_{\mathrm{hnf}}}{k_{\mathrm{f}}}\Theta'(0).
\end{aligned} \tag{14}$$

3. HAM solution

In recent years, the HAM has become a significant mathematical tool for solving complex fluid flow problems. The approach is designed to find approximate solutions to nonlinear partial differential equations that are commonly encountered in fluid dynamics using a systematic and efficient approach. Nonlinear terms in equations are handled without linearization, a common limitation in many traditional analytical methods, and this is one of the key advantages of the HAM. A more precise representation of the flow dynamics is achieved in this way, particularly in cases where nonlinearities have a significant impact on the system's behavior. The HAM's versatility makes it a valuable tool for analyzing a wide range of fluid flow problems by allowing for the inclusion of various physical parameters and boundary conditions. The fluid's behavior is influenced by multiple factors, which is why flexibility is crucial for investigating real-world scenarios. Furthermore, converging series solutions provided by the HAM are easily truncated to obtain precise approximations of the solutions. Compared with numerical techniques that may require significant computational resources, this method for solving fluid flow problems is computationally efficient.

4. Results and discussion

Casson HNFs, specifically those based on CNTs, have received a lot of attention recently due to their potential use in drug delivery systems. CNTs are a popular choice because of their exceptional characteristics such as high aspect ratio, mechanical strength and thermal conductivity. This investigation studied the flow of CNT-based HNFs on a Riga stretching plate in the presence of an electromagnetic field and double diffusion, which introduces complexity with external forces

affecting the flow behavior of HNFs. Drug delivery applications will benefit greatly from our findings because controlled flow of HNFs can be utilized to optimize the distribution and release of drugs in the body. Figure 1 shows the geometry of the proposed model and Fig. 2 the stepwise HAM solution. The delivery of therapeutic agents to specific target sites with high-precision drug delivery systems is modeled by tuning the parameters M, E, β, Ec, $\phi_1+\phi_2$, γ_e, γ_m, α and Nt, Nb, Sc, χ, k_1. The results obtained from changing parameters for the velocity, temperature and concentration profiles are displayed in figures and tables.

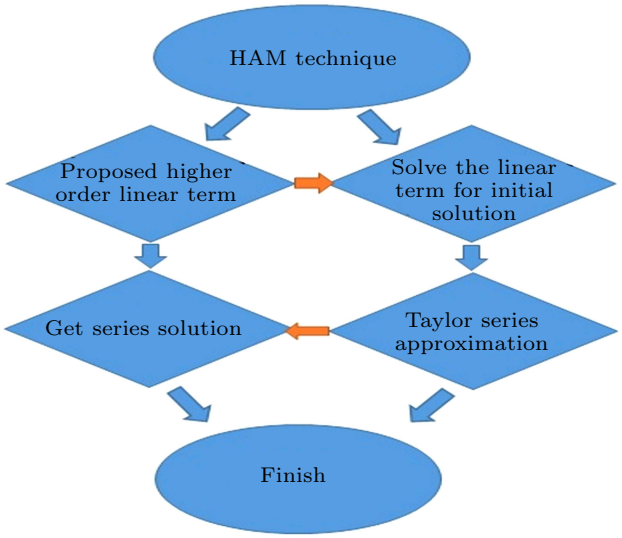


Fig. 2. The chart which shows the main steps of solution using the homotopy analysis method (HAM).

4.1. Velocity profile $f'(\eta)$

The Hartmann number α is a dimensionless number used to determine the relative importance of viscous forces compared with inertial forces in a fluid flow system, and its impact is displayed in Fig. 3(a). According to the results, the inclusion of CNTs in drug delivery systems leads to an enhancement of the velocity profile and improved drug delivery efficiency due to the increase in the value of the Hartmann number. The Casson fluid model is typically employed in drug delivery systems, and the influence of the Casson fluid parameter β can be seen in Fig. 3(b). When CNTs are used as carriers for drug delivery, the flow performance of the Casson fluid is enhanced even more. The velocity profile of the fluid flow is influenced by increasing β in the presence of CNTs. A more prominent shear-thinning behavior is observed when β is increased, and the fluid becomes less viscous at high shear rates. The result of this is faster flow rates and enhanced drug dispersion within the fluid. The velocity profile of drug transport through porous media is significantly affected by the parameter Fr, as shown in Fig. 3(c). The flow behavior within the porous medium is modified by CNTs, as well as enhancing permeability. The flow direction and velocity distribution within the medium are also altered by CNTs. Their unique structure and high aspect ratio result in a more uniform distribution $f'(\eta)$ of the drug throughout the system. CNT-based HNFs display substantial variations in flow behavior when a magnetic field parameter M is applied, as shown in Fig. 3(d). Variations in fluid viscosity and rheological properties are caused by magnetic fields acting on HNFs. Magnetic fields generate magnetic forces that affect the dispersion and stability of CNTs in the nanofluid. The alignment and dispersion of CNTs are enhanced by increasing the magnetic field strength, which improves the flow characteristics of the nanofluid, enabling targeted delivery to specific tissues or organs by facilitating better control over the drug delivery process. However, the resistive behavior of magnetic parameters controls the fluid distribution. The flow behavior of CNT-based nanofluids is

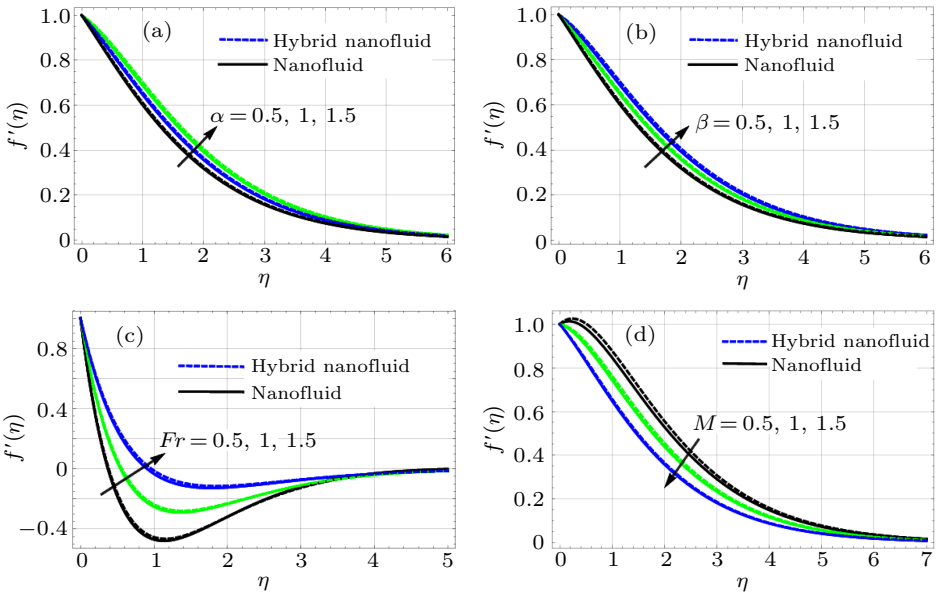


Fig. 3. Influence of (a) Hartmann number α, (b) Casson fluid parameter β, (c) parameter Fr, and (d) magnetic field parameter M on velocity field $f'(\eta)$.

crucially influenced by the electric field parameter, as shown in Fig. 3(e). The movement of CNTs within the nanofluid is triggered by electro-kinetic effects caused by electric fields, such as electrophoresis and electro-osmosis. Enhanced dispersion and mobility are achieved by increasing the intensity of the electric field and strengthening the electro-kinetic forces acting on the CNTs. By promoting a uniform distribution of drug-loaded CNTs throughout the nanofluid, the efficiency of drug delivery is enhanced. Figure 3(f) displays the impact of the volume fraction $\phi_1 + \phi_2$ of CNTs on the drug delivery system. Drug delivery is affected by the presence of CNTs, which increase resistance to flow and control drug transport. With faster and more efficient delivery of drugs, the patient's therapeutic outcome is enhanced.

4.2. Temperature profile $\Theta(\eta)$

In fluid flow, the Eckert number measures the ratio of kinetic energy to enthalpy through a dimensionless parameter. The Eckert number Ec is vital for the temperature distribution and the efficiency of drug delivery when using a CNT-based HNF for drug delivery applications, as displayed in Fig. 4(a). A higher ratio of kinetic energy to enthalpy is specified by an increase in the Eckert number, showing that convective heat transfer controls conductive heat transfer within the fluid flow. CNT-based HNFs place more stress on temperature distribution than thermal conductivity. To ensure the stability of therapeutic agents and prevent thermal degradation it is vital to control the temperature distribution when considering drug delivery applications. The temperature distribution within the nanofluid is influenced by the increased convective heat transfer caused by a higher Ec. The local temperature rise within the nanofluid can be reduced by enhanced cooling effects. Additionally, the dispersion of therapeutic agents within the nanofluid is enhanced by the increased convective heat transfer caused by a higher Ec. Optimizing Ec is vital for balancing the desired convective heat transfer effects with practical considerations such as energy consumption and system stability. The effectiveness of drug delivery processes is enhanced by a higher Ec, which promotes convective heat transfer and improves temperature control, drug stability and uniformity of drug distribution within the HNF. More efficient heat transfer throughout the system is attained by increasing the heat absorption and emission parameter χ, as shown in Fig. 4(b). Increasing χ raises the temperature of the HNF, which allows better transport of drug molecules through the system. The improved heat transfer results in better drug delivery rates and more precise drug release at the target site. Furthermore, the increased heat emission parameter χ ensures that the extra heat generated during the process is efficiently dissipated, keeping the drug molecules stable and preventing overheating. The movement of particles in a fluid due to a temperature gradient is known as thermophoresis, and the impact of the thermophoretic parameter Nt is shown in Fig. 4(c). The temperature profile for drug delivery applications is affected by the increase in the thermophoretic parameter in a Casson–CNT HNF flow. Enhanced heat transfer within the HNF is achieved by increasing Nt, which leads to a greater temperature difference across the fluid. Drug delivery applications benefit from this as it maintains the specific temperature range needed for drug stability or activation. The flow behavior of the Casson–CNT HNF is influenced by an increase in Nt, which results in changes in the velocity and temperature profiles within the flow.

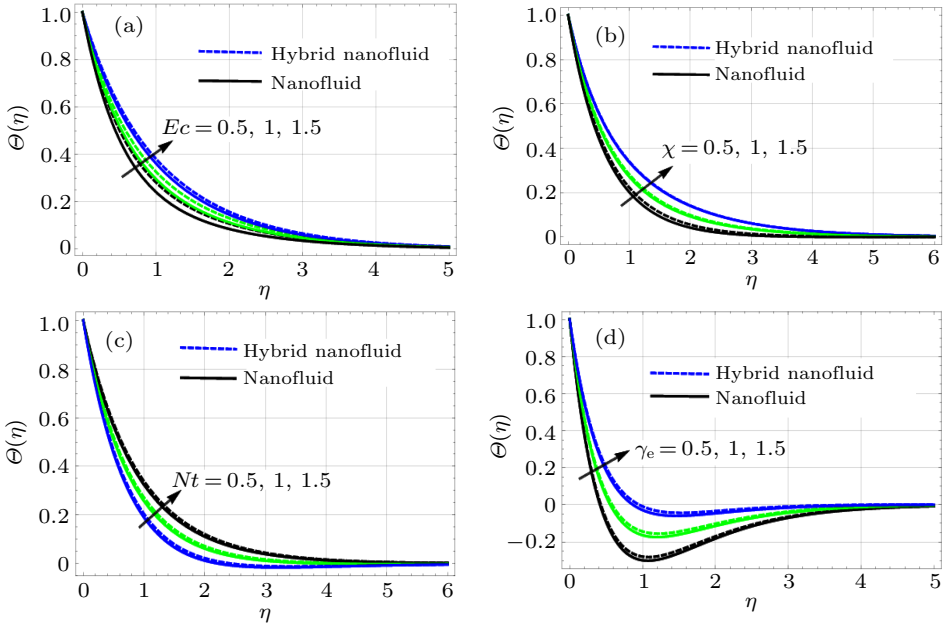


Fig. 4. Influence of (a) the Eckert number Ec, (b) the heat absorption and emission parameter χ, (c) the thermophoretic parameter χ, and (d) the thermal relaxation time parameter γ_e on the thermal profile $\Theta(\eta)$.

In this context, it is important to pay attention to the thermal relaxation time parameter γ_e displayed in Fig. 4(d). This is the time it takes for a system to return to thermal equilibrium after a temperature disturbance. The temperature profile of the Casson–CNT HNF flow is significantly affected by increasing the value of γ_e. Increasing γ_e results in a longer time for the system to reach thermal equilibrium after a temperature change. A stable temperature profile throughout the drug delivery process is achieved by the fluid's slower response to changes in temperature.

4.3. Concentration profile $\varphi(\eta)$

The Schmidt number *Sc* is a dimensionless number that explains the difference between momentum and mass diffusivity in a fluid flow. The concentration profile of the flow is significantly affected by an increase in *Sc* in Casson–CNT HNFs used for drug delivery applications, as shown in Fig. 5(a). An increase in *Sc* results in an increase in the momentum diffusivity of the fluid relative to its mass diffusivity. The capacity of the fluid to transport momentum is greater than that for mass, which results in changes in the complete flow dynamics and temperature distribution within the system. The behavior of the HNFs is influenced by the concentration relaxation time parameter, particularly in terms of effectiveness of drug delivery. As the parameter γ_e increases, the concentration profile of the Casson–CNT HNF shows changes that have a direct impact on the drug delivery process, as shown in Fig. 5(b). The HNF responds more slowly to changes in the concentration gradients when this parameter increases. The drug delivery rate is slowed because the HNF may take longer to reach a steady-state concentration distribution.

Casson–CNT HNFs employed in drug delivery applications depend on Brownian diffusivity to regulate their concentration profile. Figure 5(c) shows the changes in the concentration profile as the Brownian parameter *Nb* increases. The random motion of nanoparticles suspended in the fluid is enhanced by an increase in Brownian diffusivity. The nanoparticles are more effectively dispersed throughout the fluid medium due to increased agitation. Consequently, the concentration gradient between the drug-laden HNF and the adjacent environment becomes sharper, leading to faster diffusion of the drug molecules from the HNF to the targeted tissues or cells. The concentration profile is greatly influenced by the chemical reaction parameter k_1 in Casson–CNT HNFs used for drug delivery applications (Fig. 5(d)). The rate of chemical reactions within the nanofluid system increases when the chemical reaction parameter is increased. The stability and release kinetics of the nanoparticles are affected by this. Drug release from the nanofluid carrier decelerates depending on the chemical reactions involved. Chemical reactions can lead to faster drug release by promoting the degradation of the nanoparticle shell. The rate of drug release is decreased by reactions leading to the formation of stable complexes.

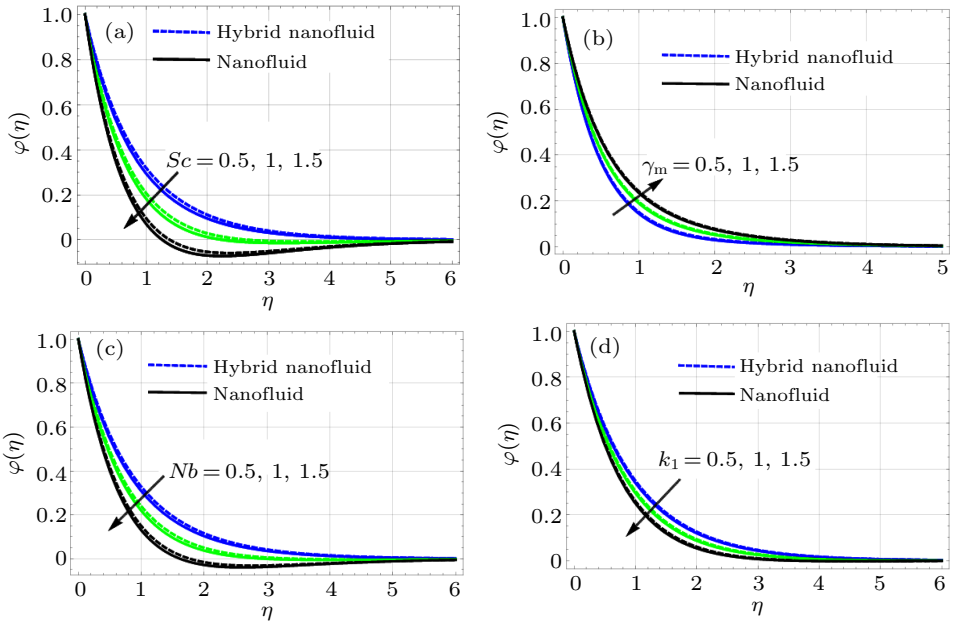


Fig. 5. Influence of (a) Schmidt number *Sc*, (b) parameter γ_m, (c) Brownian motion *Nb*, and (d) chemical reaction parameter k_1 on the concentration profile $\varphi(\eta)$.

4.4. The Nusselt number $Re_x^{-1/2}Nu$ and Sherwood number $Re_x^{-1/2}Sh$

Heat transfer and mass transfer are vital in drug delivery applications that utilize Casson–CNT HNFs as they influence the delivery system in numerous ways.

Heat transfer maintains the stability and functionality of the HNF carrier, which is vital. Thermal fluctuations are common for Casson–CNT HNFs during transport. Operative heat transfer mechanisms stop temperature-induced degradation of

drug molecules and ensure the stability of the carrier fluid by dissipating the heat generated by external factors within the HNF.

Various parameters, such as the magnetic field M, electric field E, porous space parameters λ and Fr, Casson fluid parameter β and the modified Hartmann number α, have an impact on the flow of a CNT HNF over a stretched Riga plate. To optimize drug delivery, it is crucial to understand the effects of these parameters (i.e., β, λ, Fr, α, M and E) on the skin friction profile, as shown in Table 3.

Table 3. Skin friction versus β, λ, Fr, α, M and E.

β	λ	Fr	α	M	E	$Re_x^{\frac{1}{2}} C_f$	
						Nanofluid	HNF
0.5	0.4	0.3	0.5	0.5		**1.214126**	**1.2392901**
0.7						1.240853	1.2627162
0.9						1.2730665	1.3082119
	0.4					**1.214126**	**1.2392901**
	0.6					1.22641	1.2481906
	0.8					1.239063	1.2592671
		0.3				**1.214126**	**1.2392901**
		0.5				1.240250	1.2691361
		0.7				1.2641324	1.28903920
			0.5			**1.214126**	**1.2392901**
			0.7			1.201059	1.2292177
			0.9			1.1921147	1.2125901
				0.5		**1.214126**	**1.2392901**
				0.7		1.241342	1.2547839
				0.9		1.2720876	1.285372
					0.5	**1.214126**	**1.2392901**
					0.7	1.187652	1.2109821
					0.9	1.1674298	1.1843522

The flow behavior of CNT HNFs is greatly influenced by the magnetic field parameter M. The heat transfer and fluid flow characteristics of the nanofluid are improved by the addition of a magnetic field, resulting in changes in the skin friction profile. Higher skin friction values are caused by an increase in M, which indicates a higher resistance to fluid flow over the stretched Riga plate. This makes controlling the distribution of drugs within the body easier in drug delivery applications.

The skin friction profile of CNT HNFs is also affected by the electric field parameter E. The friction value of the skin is changed by manipulating the flow behavior of the nanofluid using an electric field. The flow characteristics of the nanofluid are improved and the skin friction is reduced by increasing E, potentially leading to more efficient drug delivery. The same influence is observed for the modified Hartmann number α.

The skin friction profile of CNT HNFs is influenced by the porous space parameter λ and the Forchheimer number Fr. The flow dynamics of the nanofluid are influenced by λ and Fr, leading to higher skin friction on the stretched Riga plate. Adjusting these parameters can lead to more effective drug delivery by controlling the distribution of drugs within the body.

The skin friction profile of CNT HNFs is also influenced by the Casson fluid parameter β. The Casson model is frequently employed to depict the behavior of non-Newtonian fluids, and modifications to β influence the flow characteristics of the nanofluid. Increasing β can lead to higher skin friction values, indicating a higher resistance to fluid flow over the stretched Riga plate for drug delivery applications.

The homogeneity of drug dispersion within the HNF is enhanced and flow behavior is ensured, resulting in optimized drug delivery. The diffusion of drug molecules from the HNF carrier to the targeted tissues is governed by mass transfer, which impacts the concentration profile and time course of drug release. Mass transfer is intertwined with the transport characteristics of Casson–CNT HNFs, which include diffusivity, permeability and convective transport. Drug-loaded nanoparticles are transported quickly and efficiently within the HNF with enhanced mass transfer, ensuring timely delivery to the desired sites of action.

Table 4. Local Nusselt number versus $\phi_1+\phi_2$, χ, γ_e and Nt.

$\phi_1+\phi_2$	χ	γ_e	Nt	$Re_x^{\frac{-1}{2}} Nu_x$	
				Nanofluid	HNF
0.01	0.4	0.3	0.5	**1.14030**	**1.1402999**
0.03				1.143837	1.1449288
0.05				1.146962	1.149100
	0.4			**1.14030**	**1.1402999**
	0.6			1.142081	1.1441720
	0.8			1.143452	1.1462341
		0.3		**1.14030**	**1.1402999**
		0.5		1.1423458	1.14628104
		0.7		1.145094	1.14615056
			0.5	**1.14030**	**1.1402999**
			0.7	1.146054	1.1481381
			0.9	1.1486021	1.15266291

Table 5. Local Sherwood number versus Nt, Nb, Sc and γ_m.

Nt	Nb	γ_m	Sc	$Re_x^{\frac{-1}{2}} Sh_x$	
				Nanofluid	HNF
0.2	0.5	1.0	1.0	**1.1174**	**1.263411**
0.4				1.1813	1.271013
0.6				1.2361	1.2930861
	0.5			**1.1174**	**1.263411**
	0.7			1.10309	1.893219
	0.9			1.01576	2.005217
		1.0		**1.1174**	**1.263411**
		1.2		1.7263	2.012623
		1.4		2.0362	2.231602
			1.0	**1.1174**	**1.263411**
			1.2	1.0768	1.1390768
			1.4	0.8345	1.1034485

The numerical outputs for analyzing the heat transfer $Re_x^{\frac{-1}{2}} Nu_x$ are displayed in Table 4. We see that $Re_x^{\frac{-1}{2}} Nu_x$ is better for higher $\phi_1+\phi_2$, χ, γ_e and Nt. An in-depth discussion of these parameters is given with regard to temperature distribution, with the impact on the heat transfer rate being analyzed

in this table. The numerical data for $Re_x^{\frac{-1}{2}} Sh_x$ for nanoparticles are shown in Table 5. We see that $Re_x^{\frac{-1}{2}} Sh_x$ is greater with changes in Nt and γ_m while it is reduced for greater values of Nb and Sc

5. Conclusions

The current research is focused on a theoretical analysis of Casson-based HNFs using a Riga device. CNTs are used as the solid materials in HNFs consisting of SWCNTs and MWCNTs. A comparative analysis is performed by varying the different embedded parameters. The solution to the problem is obtained using the HAM technique. The main findings are obtained as follows:

The Eckert number Ec is vital in the temperature distribution and efficiency of drug delivery using CNT-based HNFs for drug delivery. By increasing Ec in HNFs, temperature distribution in the system becomes more efficient allowing targeting of the desired tissues in the drug delivery process.

Casson–CNT HNFs can enhance the efficiency and effectiveness of drug delivery systems by increasing the heat absorption parameter χ.

Overheating of the drug solution, that could potentially damage the drug molecules or the surrounding tissue, is prevented by increasing the thermal relaxation time parameter γ_e.

Drug mixing and dispersion within the HNF improves delivery efficiency by enhancing the Schmidt number Sc.

Boundary layers and stationary regions within the fluid flow are disturbed due to enhanced Brownian motion Nt.

As the modified Hartmann number α increases, the flow rate of the HNF is improved but it decreases with larger values of Fr, β, λ and M. The results for the Hartmann number of the Riga actuator can be applied when high-speed flows are required.

The skin friction of CNT HNFs flow on a stretched Riga plate for drug delivery applications is determined by the magnetic field, electric field, porous space and Casson fluid, all of which have significant roles to play in improving the performance of drug delivery.

Appendix A

Table A1. Nomenclature.

(u,v), velocity terms (m· s^{-1})	ρ_{nf}, nanofluid density (kg·m^{-3})
(x,y), coordinate axis (m)	$\alpha = \frac{j_0 M^* \pi}{8a^2 x \rho_f}$, modified Hartmann number
$f(\eta)$, velocity in dimensionless form	$\gamma_e = a\tau_e$, thermal relaxation time parameter
K, Darcy permeability (m^2)	$\lambda = \frac{\nu_f}{ak^*}$, porosity parameter
Q, heat source/sink	$M = \frac{\sigma_f B_0^2}{\rho_f a}$, magnetic field
Λ, thermophoresis coefficient	υ_{nf}, kinematic viscosity of the nanofluid (m^2·s^{-1})
D, mass diffusivity	k_{nf}, thermal conductivity of the nanofluid (W·K^{-1}·m^{-1})
C_f, skin friction	$(\rho\beta)_{nf}$, nanofluid thermal expansion (kg·m^{-3}·K^{-1})
$ax = U_w$, stretching velocity (m·s^{-1})	$Pr = \frac{\mu c p}{k_f}$, Prandtl number
k^*, mean absorption coefficient (m^{-1})	Nu, Nusselt number
β, Casson fluid parameter	μ_{nf}, dynamic viscosity of the nanofluid (kg·m·s^{-1})
T, local temperature (K)	$Ec = \frac{U_w^2}{(c_p)_f (T_w - T_\infty)}$, Eckert number
η, similarity variable	$\gamma_m = a\tau_m$, concentration relaxation time parameter
c_p, specific heat (J·kg^{-1}·K^{-1})	$Nt = \frac{\tau D_T (T_w - T_\infty)}{\upsilon_f T_\infty}$, thermophoresis parameter
σ^*, Stefan–Boltzmann constant (W·K^{-4}·m^{-2})	$Sc = \frac{\upsilon_f}{D_B}$, Schimdt number
B_0, magnetic field strength (T)	Q, heat generation/absorption parameter
$E = \frac{E_0}{B_0(U_w)}$, electric field	$\chi = \frac{Q}{(\rho c_p)_f a}$, heat generation/absorption parameter
E_0, electric field strength (V·m^{-1})	σ_{nf}, electrical conductivity of the nanofluid (S·m^{-1})
$Fr = \frac{xF_0}{\rho_f}$, Forchheimer number	$Nb = \frac{\tau D_B (C_w - C_\infty)}{\upsilon_f}$, Brownian diffusivity parameter
$\phi_{SWCN} = \phi_1$, $\phi_{MWCN} = \phi_2$, nanoparticle volume fraction	$k_1 = \frac{kr}{a}$, chemical reaction parameter

Acknowledgement

The authors extend their appreciation to the Deanship of Scientific Research at Imam Mohammad Ibn Saud Islamic University (IMSIU) for funding this work (Grant No. IMSIU-RPP2023053).

References

[1] Jin C, Wu Q, Yang G, Zhang H and Zhong Y 2021 *Powder Technology* **389** 10

[2] Gul T, Bilal M, Shuaib M, Mukhtar S and Thounthong P 2020 *Heat Transfer* **49** 3211

[3] Balaji T, Rajendiran S, Selvam C and Lal D M 2021 *Powder Technology* **394** 1141

[4] Kaur K and Jeet K 2017 *Fullerenes, Nanotubes and Carbon Nanostructures* **25** 726

[5] Zhang W, Zhang Z and Zhang Y 2011 *Nanoscale Research Letters* **6** 22

[6] Saleemi M A, Kong Y L, Yong P V C and Wong E H 2020 *Journal of Drug Delivery Science and Technology* **59** 101855

[7] Bianco A, Kostarelos K and Prato M 2005 *Current Opinion in Chemical Biology* **9** 674

[8] Rahamathulla M, Bhosale R R, Osmani R A, Mahima K C, Johnson A P, Hani U and Gangadharappa H V 2021 *Materials* **14** 6707
[9] Alharbi S O, Khalifa H A E W, Gul T, Alharbi R, Alburaikan A and Bariq A 2024 *Discover Applied Sciences* **6** 200
[10] Sarkar S and Das S 2023 *Journal of Molecular Liquids* **390** 123035
[11] Lone S A, Khan A, Gul T, Mukhtar S, Alghamdi W and Ali I 2024 *Colloid and Polymer Science* 26
[12] Naseem A, Shafiq A, Naseem F and Farooq M U 2022 *Energies* **15** 6891
[13] Upreti H, Pandey A K, Joshi N and Makinde O D 2023 *Journal of Computational Biophysics and Chemistry* **22** 321
[14] Senthilvadivu, K, Eswaramoorthi S, Loganathan K and Abbas M 2024 *Nanotechnology Reviews* **13** 20230202
[15] Baithalu R, Panda S, Pattnaik P K and Mishra S R 2024 *Int. J. Appl. Comput. Mathematics* **10** 20
[16] Zeeshan A, Shah N A and Chung J D 2023 *Mathematics* **11** 1170
[17] Ramzan M, Gul H, Malik M Y, Baleanu D and Nisar K S 2021 *Scientific Reports* **11** 19590
[18] Madkhali H A, Haneef M, El-Shafay A S, Alharbi S O and Nawaz M 2022 *Int. Comm. in Heat and Mass Transfer* **130** 105714
[19] Jiang Y, Zhang J, Abdeljawad T, Ahmad S, Naveed K M, Rehman A and El-Shafay A S 2022 *Nanomaterials* **12** 439
[20] Thabet E N, Khan Z, Abd-Alla A M, Alharbi FM, Bayones F S, Alwabli A S and Elhag S H 2024 *AIP Advances* **14** 035048
[21] Waqas H, Muhammad T, Khan S A and Yasmin S 2021 *Euro. Phys. J. Plus* **136** 860
[22] Sharma T, Kumar R and Chamkha A J 2023 *Journal of Nanofluids* **12** 1951
[23] Khashi'ie N S, Waini I, Arifin N M and Pop I 2023 *Int. J. of Numerical Methods for Heat & Fluid Flow* **33** 333
[24] Khashi'ie N S, Waini I, Wahid N S, Arifin N M and Pop I 2023 *Chinese Journal of Physics* **81** 181
[25] Nasir S, Berrouk A S, Gul T, Zari I, Alghamdi W and Ali I 2023 *Scientific Reports* **13** 10947
[26] Saeed A, Alsubie A, Kumam P, Nasir S, Gul T and Kumam W 2021 *Scientific Reports* **11** 12865
[27] Usman M, Gul T, Khan A, Alsubie A and Ullah M Z 2021 *Int. Comm. in Heat and Mass Transfer* **127** 105562
[28] Gul T, Qadeer A, Alghamdi W, Saeed A, Mukhtar S and Jawad M 2021 *Int. J. of Numerical Methods for Heat & Fluid Flow* **32** 642
[29] Liao S J 1997 *Int. J. of Non-Linear Mechanics* **32** 815
[30] Liao S J 2003 *Journal of Fluid Mechanics* **488** 189
[31] Gul T and Khan Z 2023 *City University Int. J. of Computational Analysis* **6** 1
[32] Ayed H, Mouldi A, Gul T, Mukhtar S, Ali I and Ali F 2023 *J. of Thermal Analysis and Calorimetry* **148** 12699